Performance of $La_{2-x}Sr_xCo_{0.5}Ni_{0.5}O_{4\pm\delta}$ as an Oxygen Electrode for Solid Oxide Reversible Cells[×]

M. A. Laguna-Bercero[1*#], N. Kinadjan[2], R. Sayers[1], H. El Shinawi[3&], C. Greaves[3] and S. J. Skinner[1],

[1] Department of Materials, Imperial College London, SW7 2AZ London, UK
[2] Grenoble INP, Phelma, SIMAP, F-38402 St Martin Dheres, France
[3] Univ Birmingham, Sch Chem, Birmingham B15 2TT, W Midlands, England

Received

[*] Corresponding author, malaguna@unizar.es
[#] Present address, Instituto de Ciencia de Materiales de Aragón, CSIC - Universidad de Zaragoza, Pedro Cerbuna 12, 50009 Zaragoza, Spain
[&] Present address, Chemistry Department, Faculty of Science, Mansoura University, Mansoura, Dakhalia 35516, Egypt

Abstract

$La_{2-x}Sr_xCo_{0.5}Ni_{0.5}O_{4\pm\delta}$ (LSCN) is presented as a novel electrode for both Solid Oxide Fuel Cells (SOFC) and Solid Oxide Electrolysis Cells (SOEC). LSCN/10Sc1CeSZ (scandia and ceria stabilized zirconia)/ LSCN symmetrical cells were fabricated and characterized by AC impedance spectroscopy under different oxygen partial pressures at temperatures of up to 900ºC. At 850 ºC polarization resistances of 5.15 Ωcm^2 and 5.74 Ωcm^2 were found applying air and oxygen, respectively. Electrolysis and fuel cell *j*-V experiments were also performed at temperatures between 700 ºC and 850 ºC using a LSCN/ 10Sc1CeSZ/ Ni-YSZ. Electrochemical results showed that the cell performs equally in both SOFC and SOEC modes. Detailed results in terms of performance are presented and discussed. LSCN is presented as a good candidate for both SOFC and SOEC. The similar performance obtained for *j*-V (current density-voltage) curves in electrolysis and fuel cell operation mode is thought to be related to the flexible oxygen nonstoichiometry of the LSCN (K_2NiF_4-type structure).

Keywords: K_2NiF_4 structure, oxygen non-stoichiometry, zirconia, SOFC, SOEC, hydrogen production

1 Introduction

The development of Solid Oxide Fuel Cells (SOFCs) and Solid Oxide Electrolysis Cells (SOECs) for operation at intermediate temperatures (500 ºC to 750 ºC) has potentially significant engineering advantages, such as the easy sealing between the materials and a decrease of interdiffusion between cell components. One of the major problems in SOFCs, particularly at intermediate temperatures (IT), is the large cathode overpotential during operation [1,2]. Up to 60% of voltage loss in anode-supported SOFCs can occur at the cathode due to polarization losses associated with the oxygen reduction reaction [3]. The majority of SOFC cathodes to date are based upon either $LaMnO_3$ or $LaCoO_3$ perovskite-type materials substituted with Sr on the A-site and Fe on the B-site.

Lanthanide nickelates (Ln = La, Nd, Pr) have received considerable interest as materials for IT-SOFC electrodes and oxygen separation membranes [4,5,6]. These materials present a K_2NiF_4-type structure consisting of alternate $LnNiO_3$ perovskite layers and LnO rock-salt layers with excess oxygen atoms occupying the interstitial sites between the LnO layers. $Ln_2NiO_{4\pm\delta}$ materials belong to the Ruddlesden-Popper series and present flexible oxygen stoichiometry, leading to fast oxygen ion diffusion through

[×] Article is part of "Special issue Albacete 2009"

bulk materials and rapid surface exchange kinetics. They can accommodate intestitial oxygen excess under high pO_2 atmospheres, and also can withstand low pO_2 atmospheres *via* loss of oxygen, generating oxygen substoichiometric phases [7]. $La_2NiO_{4+\delta}$, the parent compound, presents an electronic conductivity of ~100 S cm^{-1} at 800 ºC [8] and the oxide-ion conductivity is also higher than the conventional perovskites [4]. Another advantage of these Ruddlesden-Popper type materials in addition to the high oxygen mobility is the relatively low lattice expansion induced by variations in temperature and oxygen partial pressure [9]. For implementation of these materials in devices their phase stability is of great importance at temperatures up to 1000 ºC and over a wide pO_2 range. Some authors have also reported their good chemical and mechanical stability with YSZ (yttria stabilized zirconia) [10] but Echigoya *et al.* have also found an increase in the resistivity in La_2NiO_4 films deposited on YSZ above 1000 ºC, due to the formation of the insulating $La_2Zr_2O_7$ [11]. Other authors have also found problems of chemical stability and electrolyte incompatibility [12,13]. Thermodynamic modelling calculations made by Solak *et al.* [14] also showed that $La_2NiO_{4+\delta}$ is not chemically compatible with the LSGM electrolyte at fabrication and operation conditions. On the contrary, Sayers *et al.* [15] recently found that there was no evidence of secondary phase formation in $La_2NiO_{4+\delta}$-LSGM mixtures, and they also found that there was significant reactivity between $La_2NiO_{4+\delta}$ and CGO after 24h at 900 ºC, with the formation of a higher order Ruddlesden-Popper ($La_{n+1}Ni_nO_{3n+1}$) phase as one of the reaction products.

Previous studies on K_2NiF_4 type phases [16,17,18] suggested that the introduction of M^{3+} ions into the B-site compensated by Sr doping on the A-site may improve the phase stabilitity of $La_{2-x}Sr_xCo_{0.5}Ni_{0.5}O_{4\pm\delta}$ by the formation of stable B-site cations under oxidizing conditions where the material presents an oxygen excess phase. Moreover, relatively stable oxygen-deficient phases could be obtained under reducing conditions due to the reduction of Co^{3+} to Co^{2+}. However, there are no reports of the electrochemical performance of these oxygen deficient phases in single or symmetrical cells. By contrast, there are many reports of the performance of oxygen-excess phases in SOFC mode and recently, similar materials such as $Nd_2NiO_{4+\delta}$ have been proposed as good candidates especially in SOEC mode [19]. It is likely that these materials have shown good performance due to the range of possible oxygen non-stoichiometries that this structure type can adopt. We believe that the capability of these materials to accommodate oxygen excess will favor the catalytic activity of these electrodes in SOEC mode for oxygen evolution. During the steam electrolysis high oxygen partial pressures occur at the electrode/electrolyte interface and delamination of oxygen electrodes, due to these high oxygen pressures at the interface, is one of the major problems in SOEC [20,21]. The use of electrodes based on the LSCN system, with a high range of oxygen stoichiometries, may improve their phase-stability and the electrode/electrolyte interface under high oxygen partial pressures during SOEC operation.

We have therefore focused on the system $La_{2-x}Sr_xCo_{0.5}Ni_{0.5}O_{4\pm\delta}$ (LSCN), in particular on the $La_{1.7}Sr_{0.3}Co_{0.5}Ni_{0.5}O_{4.08}$ hyperstoichiometric phase where oxygen excess is located in the interstitial sites [22]. The material presents enhanced phase-stability under both oxidizing and reducing conditions in comparison with $La_2NiO_{4+\delta}$ and $La_2Ni_{1-x}Co_xO_{4+\delta}$ [22]. In addition, mixed transition metal valency ($(Co/Ni)^{2+/3+}$) provides good mixed conducting properties for these materials. The overall conductivity at elevated temperatures has been reported as greater than 100 S cm^{-1} [22] and the material has potential in applications as the oxygen electrode in both SOFC and SOEC modes of operation.

2 Experimental

$La_{1.7}Sr_{0.3}Co_{0.5}Ni_{0.5}O_{4(+\delta)}$ was synthesized by a sol-gel procedure using stoichiometric amounts of $SrCO_3$, La_2O_3, $Ni(CH_3COO)_2.4H_2O$ and $Co(CH_3COO)_2.4H_2O$, as described in [22]. In this study, dense electrolyte pellets were fabricated using 10Sc1CeSZ (10% Sc_2O_3 and 1%CeO_2 doped ZrO_2) powder (Fuel Cell Materials Inc). The powder was ball milled for 48 hours in acetone, dried, and then pressed into pellets of 13mm in diameter and thickness of about 2 mm, applying 20 MPa of uniaxial pressure and followed by isostatic pressing at 300MPa. The pellets were then sintered at 1500°C for 24 hours and quenched to room temperature from 1000 ºC to avoid the formation of the rhombohedral phase $Sc_2Zr_2O_7$ [23]. Inks were prepared from the LSCN powder and a commercial ink vehicle (Fuel Cell Materials Inc.)

with a final composition of 67wt% of powder using a triple-roll mill. The ink was then screen-printed on both sides of the 10Sc1CeSZ pellet, and sintered at 1000 ºC for two hours. The sample was then mounted in a spring-loaded jig using Pt mesh as the current collector. AC impedance measurements were recorded using a Solartron 1260 impedance analyser in the frequency range of 10MHz to 0.1 Hz using an electrical perturbation of 50 mV. The data obtained were then analysed with the ZView software [24].

Ni-YSZ (electrode)/10Sc1CeSZ (electrolyte) half-cells provided by Kerafol Gmbh, Germany were used for the electrochemical experiments. The pellets consist of 10% Sc_2O_3 – 1% CeO_2 – ZrO_2 (10Sc1CeSZ) electrolyte (mol%) of 20 mm diameter and 155 ± 5 µm thickness, and nickel- 8% Y_2O_3 – ZrO_2 (YSZ) electrolyte (mol%) of ~40 µm thickness. LSCN deposited by screen-printing was used as the oxygen electrode and the final thickness was ~10 µm. The experimental setup for the fuel cell/electrolysis experiments is described in detail in reference [25]. Synthetic air was supplied to the oxygen electrode side and the fuel electrode was fed with hydrogen (96%) and water vapour (4%), both using mass flows of 200 ml/min. Electrochemical impedance spectroscopy (EIS), and potentionstatic/potentiodynamic experiments were performed using an Autolab PGSTAT30 fitted with a frequency response analyser (FRA) (Autolab, EcoChemie, Netherlands). Impedance measurements under potential load were performed in potentiostatic mode using a sinusoidal signal amplitude of 50 mV over the frequency range of 10 kHz to 0.1 Hz.

3 Results and discussion

$La_{1.7}Sr_{0.3}Co_{0.5}Ni_{0.5}O_{4.08}$ powder has been confirmed to crystallise as a single phase that adopts the tetragonal I4/mmm space group consistent with the K_2NiF_4-type structure. Detailed discussion of the structure determination and characterisation of this composition can be found in reference [22]. Previous studies of LSCN in contact with YSZ [26] had indicated good compatibility of the LSCN with fluorite type electrolytes. However ScSZ has higher ionic conductivity at lower temperature (IT-SOFC regime) and as such this electrolyte has been selected for the current study.

For the symmetrical cell and for the electrochemical experiments we have chosen the 10Sc1CeSZ electrolyte due to its higher ionic conductivity in comparison with the standard YSZ. In order to obtain a good interface between the LSCN and the zirconia electrolyte a range of sintering temperatures between 900 and 1100 ºC were studied, and it was observed that best conditions were sintering at 1000 ºC for 2 hours. The microstructure of the electrode layer produced is shown in Figure 1. Good adherence is shown between both phases (Figure 1a). The thickness of the electrode layer is around 10 µm. In Figure 1b we observe a homogeneous distribution of particles and pores that will assure adequate electronic conductivity and fluent gas transport during operation. Particle size and pore size distributions were calculated from the SEM images, with particle sizes determined to be in the range of 200nm to 600 nm and pore sizes between 200 nm and 1 µm. No reactivity between the LSCN and the 10Sc1CeSZ phases was found by XRD.

Electrode performance of the LSCN was evaluated through the measurement of LSCN/10Sc1CeSZ/LSCN symmetrical cells using EIS. In Figure 2 we present Nyquist plots recorded at different temperatures under air (Figure 2a) and under pure oxygen (Figure 2b). The data were fitted using the equivalent circuit shown as an inset in Fig 2 and the resistances, capacitances, characteristic frequencies and ASR (area specific resistance) values obtained from the fitting are shown in table 1. Two processes, one at intermediate frequencies (~10-20 kHz) and another at low frequencies (~200-400 Hz) are clearly observed. According with the capacitance values and also considering the standard interpretation for electroceramics in the literature [27], the intermediate frequency arc is associated with oxygen transfer at the LSCN/10Sc1CeSZ interface and the arc at low frequencies is most likely due to the oxygen reduction reaction (surface diffusion of oxygen ions, oxygen adsorption, dissociation, etc.). These results are in concordance with previous studies in the literature, especially to those related to the parent $La_2NiO_{4+\delta}$ compound [28,29]. It is also remarkable that the response under air atmosphere is very similar to that under pure oxygen, especially at higher temperatures. This is probably a consequence of the good oxygen diffusion for the LSCN electrode at the measured temperatures, even at intermediate oxygen

partial pressures (pO_2 = 0.21 atm), as under pO_2 equal to 1 atm a clear enhancement is expected that is not observed. The ASR values are still far from those usually considered for SOFC and SOEC applications (under 1 Ωcm^2) due to a non-optimized microstructure for the interface between the LSCN electrode and the 10Sc1CeSZ electrolyte. Although the LSCN microstructure and also the LSCN/10Sc1CeSZ interface seem adequate from examination of the SEM micrographs (Figure 1), optimizing the microstructure by addition of functional layers and also using composite electrodes, will help to improve the adherence between phases and as a consequence, ASR values will be reduced. For example, it was found that for the $La_2NiO_{4+\delta}$ electrode, ASR values can be drastically reduced from 6 Ωcm^2 to 0.11 Ωcm^2 by optimizing the microstructure [28]. The aim of the present study was to demonstrate the suitability of the LSCN as an oxygen electrode for both SOFC and SOEC applications, and not optimizing the electrode/electrolyte interface. Further experiments are required in order to optimize the interface.

j-V curves (potentiodynamic mode) in both SOFC and SOEC modes of operation are plotted in Figure 3 for temperatures of between 700 ºC and 850 ºC for a Ni-YSZ/10Sc1CeSZ/LSCN single cell. It is remarkable that for j = -0.4 Acm^{-2}, relatively high fuel utilization (~38%) is achieved in SOEC mode due to the low steam concentration supplied to the fuel electrode side, and concentration polarization losses were not observed. However in fuel cell mode significantly lower fuel utilization was observed (around 2%).

ASR values obtained from the slope of the *j*-V curves are also presented in table 2. At higher temperatures (800-850 ºC), the cell is performing equally in both operation modes (ASR values at 850ºC were 1.92 Ωcm^2 and 2.05 Ωcm^2 for SOFC and SOEC respectively). This effect is also clearly observed at higher temperatures from the AC impedance experiments performed under potential load (Figure 4), where the polarization resistances under a bias potential of ±0.5V are almost identical. On the contrary, at lower temperatures (700 ºC), lower ASR values were obtained under electrolysis mode (2.60 Ωcm^2) in comparison with those obtained under SOFC mode (4.13 Ωcm^2). In electrolysis mode, there is an increase of pO_2 at the oxygen electrode/ electrolyte interface due to the oxygen evolution. The hyperstoichiometry of the LSCN phase is probably the reason for the good oxygen evolution, as also previously observed for the $Nd_2NiO_{4+\delta}$ electrode [19]. It is also remarkable that the results of the SOEC experiments were obtained at low steam partial pressure (pH_2O = 0.03 atm), and we would expect even lower ASR values at higher steam concentrations, especially at high current densities.

Finally, activation for the LSCN electrode was observed under polarization, especially after *j*-V experiments in SOEC mode. AC impedance data were recorded prior to the *j*-V SOEC curves, immediately after these experiments and also up to two hours after, as presented in Figure 5. This polarization is also observed after SOFC polarization, although in this case the effect is less noticeable and initial polarization is recovered after a much shorter time (less than 10 minutes), and not after more than two hours as observed subsequent to SOEC polarization. It is well known that cathodic current passage enhances the polarization performance of LSM cathodes for O_2 reduction [30,31]. Baumann *et al.* [32] also studied the polarization resistance of mixed conducting SOFC cathodes using thin films, and they found that a cathodic dc voltage treatment with about 1-3V for up to a few minutes leads to a drastic decrease of the impedance of Co-rich $La_{0.6}Sr_{0.4}Co_{1-x}Fe_xO_{3-\delta}$ (LSCF) electrodes. On the contrary, in Fe-rich LSCF compounds as well as in $Ba_{0.5}Sr_{0.5}Co_{0.8}Fe_{0.2}O_{3-\delta}$ and $Sm_{0.5}Sr_{0.5}CoO_{3-\delta}$ minor or negligible activation effects were found. The authors observed Co and Sr enrichment in the surface region upon cathodic treatments that would contribute to this effect. A similar behaviour is now observed in our sample for the first time on K_2NiF_4 phase-based materials, also containing a Co-rich phase. Further experiments are required in order to identify the origin of this effect, although the origin seems to be similar to that observed for the LSCF.

4 Summary

$La_{1.7}Sr_{0.3}Co_{0.5}Ni_{0.5}O_{4.08}$ is proposed as a novel oxygen electrode for both SOFC and SOEC applications as the material presented no reaction with the 10Sc1CeSZ electrolyte. AC impedance measurements on symmetrical LSCN/10Sc1CeSZ/LSCN cells showed at 850 ºC ASR values of 5.15

Ωcm^2 and 5.74 Ωcm^2 in both air and oxygen atmospheres, respectively. Two processes were observed from these measurements. The intermediate frequency arc is most likely associated with oxygen transfer at the LSCN/10Sc1CeSZ interface and the arc at low frequencies is most likely due to the oxygen reduction reaction. In addition, *j*-V experiments (both fuel cell and electrolysis mode) were also performed in a LSCN/ 10Sc1CeSZ/ Ni-YSZ single cell. At higher temperatures (800-850 ºC), the cell seems to perform equally in both operation modes. ASR values at 850ºC were 1.92 Ωcm^2 and 2.05 Ωcm^2 for SOFC and SOEC respectively. On the contrary, at lower temperatures (700 ºC), lower ASR values were found under electrolysis mode in comparison with SOFC mode. Finally, activation for the LSCN electrode was observed after SOEC polarization, possibly due to cobalt enrichment in the surface region. The hyperstoichiometry of the LSCN phase is probably the cause for the good oxygen evolution in SOEC mode.

Acknowledgments

We would like to thank UKERC (NERC-TSEC programme grant number: NE/C516169/1) and INPG for funding a studentship (NK). We also thank Prof. Nigel Brandon's group in the Department of Earth Science Engineering, Imperial College London, for the use of their facilities to carry out the electrochemical experiments.

Figure Captions

Fig. 1 SEM micrographs (transverse cross section, fracture view) for the LSCN electrode (a) and the LSCN/10Sc1CeSZ interface

Fig. 2 Nyquist plots recorded at different temperatures under air (a) and under pure oxygen (b) for the LSCN/10Sc1CeSZ/LSCN symmetrical (electrolyte supported) cell

Fig. 3 *j*-V curves in both SOFC and SOEC mode recorded at different temperatures for the electrolyte supported Ni-YSZ/10Sc1CeSZ/LSCN single cell.

Fig. 4 Nyquist plots recorded at 800 ºC (a) and 850 ºC (b) for the Ni-YSZ/10Sc1CeSZ/LSCN single cell at OCV and also under a bias potential of +0.5V and -0.5V vs. OCV.

Fig. 5 Nyquist plots recorded at 750 ºC before and after SOEC polarization. All impedance spectra were recorded at OCV which was constant at 0.994 V.

Tables

Table 1 Impedance parameters (resistances, capacitances, characteristic frequencies and total ASR values) obtained for the LSCN/10Sc1CeSZ/LSCN symmetrical cell at different temperatures under air and oxygen atmosphere by fitting of the experimental data.

pO_2 (atm)	Temp. (ºC)	ASR (Ωcm^2)	R_1 (Ω cm^2)	C_1 (F cm^{-2})	f_1 (kHz)	R_2 (Ω cm^2)	C_2 (F cm^{-2})	f_2 (Hz)
0.21	700	27.38	13.28	5.91 x 10^{-6}	1.8	14.1	7.03 x10^{-5}	92
0.21	750	16.03	7.16	2.72 x 10^{-6}	4.6	8.87	4.08 x10^{-5}	230
0.21	800	9.01	3.60	1.36 x 10^{-6}	7.5	5.41	2.58 x10^{-5}	517
0.21	850	5.15	1.59	1.33 x 10^{-6}	30.0	3.56	2.06 x10^{-5}	1430
1	700	25.31	12.28	4.80 x 10^{-6}	1.8	13.03	8.69 x10^{-5}	82
1	750	15.07	6.55	2.74 x 10^{-6}	4.5	8.52	5.69 x10^{-5}	206

1	800	9.89	4.01	1.61 x 10^{-6}	7.3	5.88	3.97 x10^{-5}	366
1	850	5.74	2.26	1.34 x 10^{-6}	11.0	3.48	3.00 x10^{-5}	651

Table 2. ASR values obtained from the slope of the *j*-V curves for the LSCN/10Sc1CeSZ/Ni-YSZ cell at different temperatures under pO_2 = 0.21 atm supplied to the oxygen electrode and pH_2O = 0.03 atm and pH_2 = 0.97atm supplied to the fuel electrode.

Temp. (ºC)	**ASR (Ωcm^2) SOFC mode**	**ASR (Ωcm^2) SOEC mode**
700	4.13±0.06	2.60±0.01
750	2.80±0.02	2.36±0.01
800	2.52±0.02	2.25±0.01
850	1.92±0.01	2.05±0.02

Table 3. Ohmic resistances (R_{ohm}) and polarization resistances (R_{pol}) obtained from the fitting of the AC impedance experiments under different polarization conditions for the LSCN/10Sc1CeSZ/Ni-YSZ cell at 800 and 850 ºC.

Temp. (ºC)	**Polarization**	**R_{ohm} (Ωcm^2)**	**R_{pol} (Ωcm^2)**
800	OCV	0.21±0.01	1.99±0.01
800	OCV -0.5V	0.19±0.01	0.30±0.01
800	OCV +0.5V	0.19±0.01	0.33±0.01
850	OCV	0.16±0.01	1.75±0.02
850	OCV -0.5V	0.17±0.01	0.42±0.01
850	OCV +0.5V	0.16±0.01	0.38±0.01

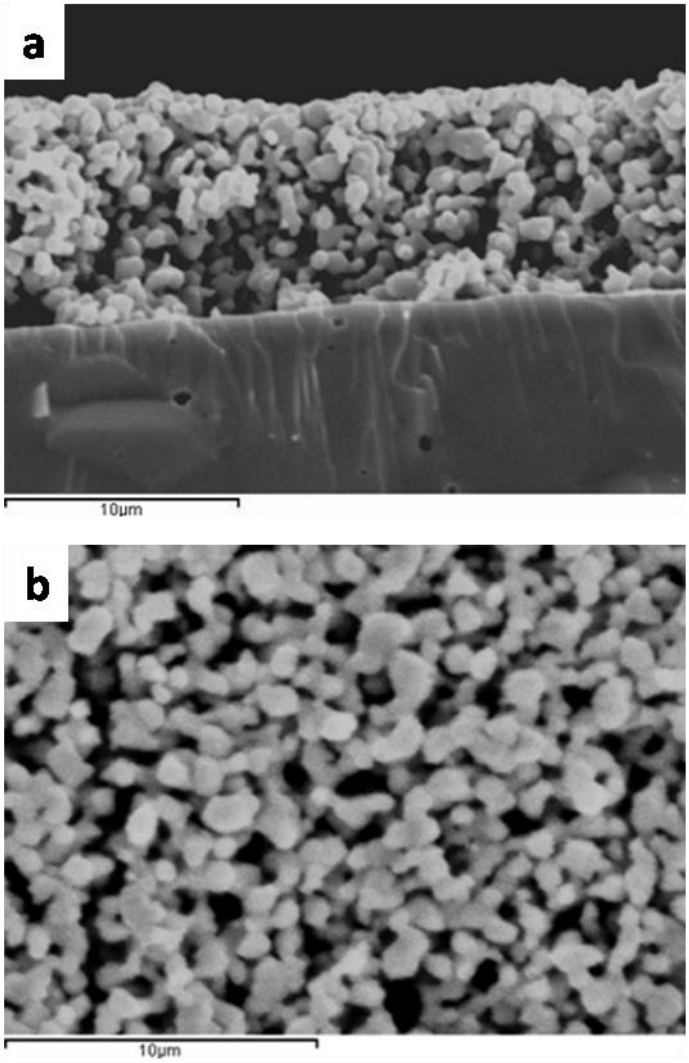

Figure 1

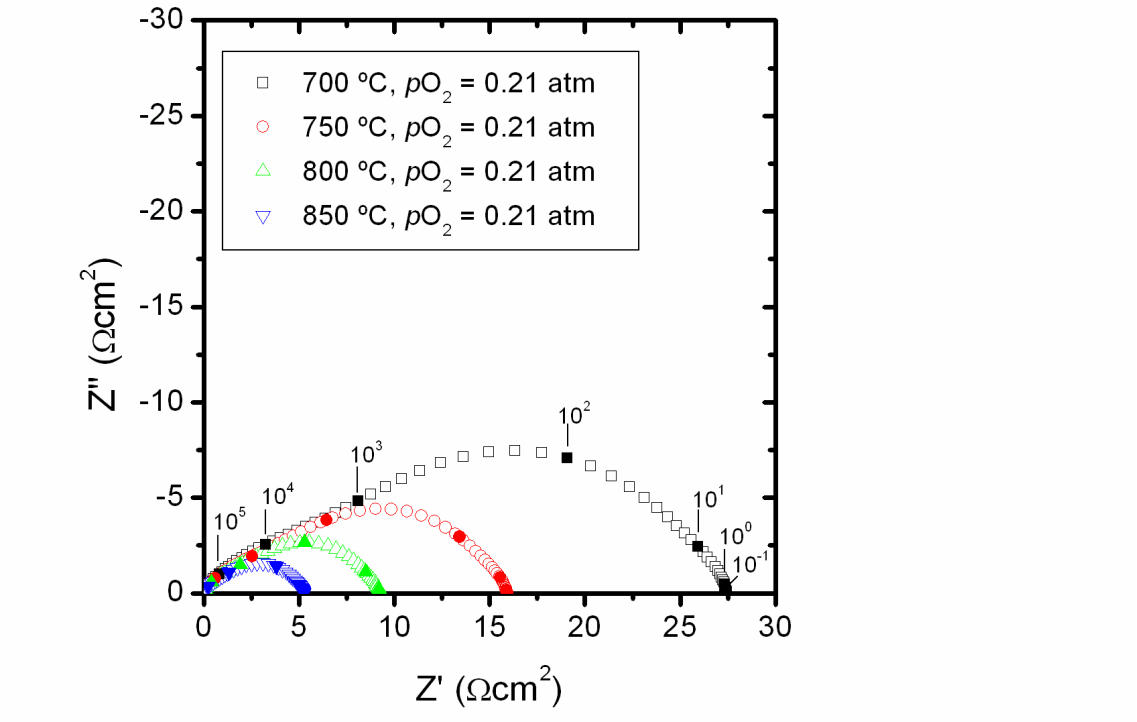
700 °C, pO2 = 0.21 atm
750 °C, pO2 = 0.21 atm
800 °C, pO2 = 0.21 atm
850 °C, pO2 = 0.21 atm
Z'' (Ωcm2)
Z' (Ωcm2)
-30
-25
-20
-15
-10
-5
0
0
5
10
15
20
25
30
10^5
10^4
10^3
10^2
10^1
10^0
10^-1

Figure 2a

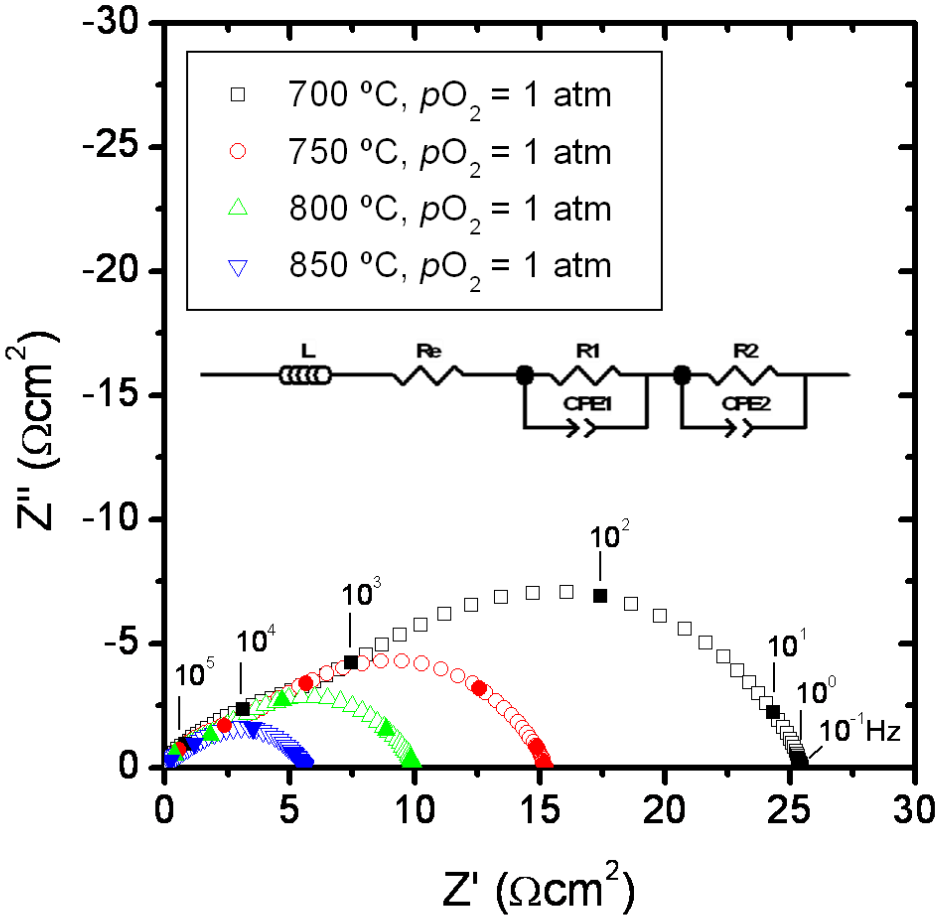
700 ºC, pO2 = 1 atm
750 ºC, pO2 = 1 atm
800 ºC, pO2 = 1 atm
850 ºC, pO2 = 1 atm
L
Re
R1
R2
CPE1
CPE2
10^2
10^3
10^4
10^5
10^1
10^0
10^-1 Hz
Z'' (Ωcm^2)
Z' (Ωcm^2)
-30
-25
-20
-15
-10
-5
0
0
5
10
15
20
25
30

Figure 2b

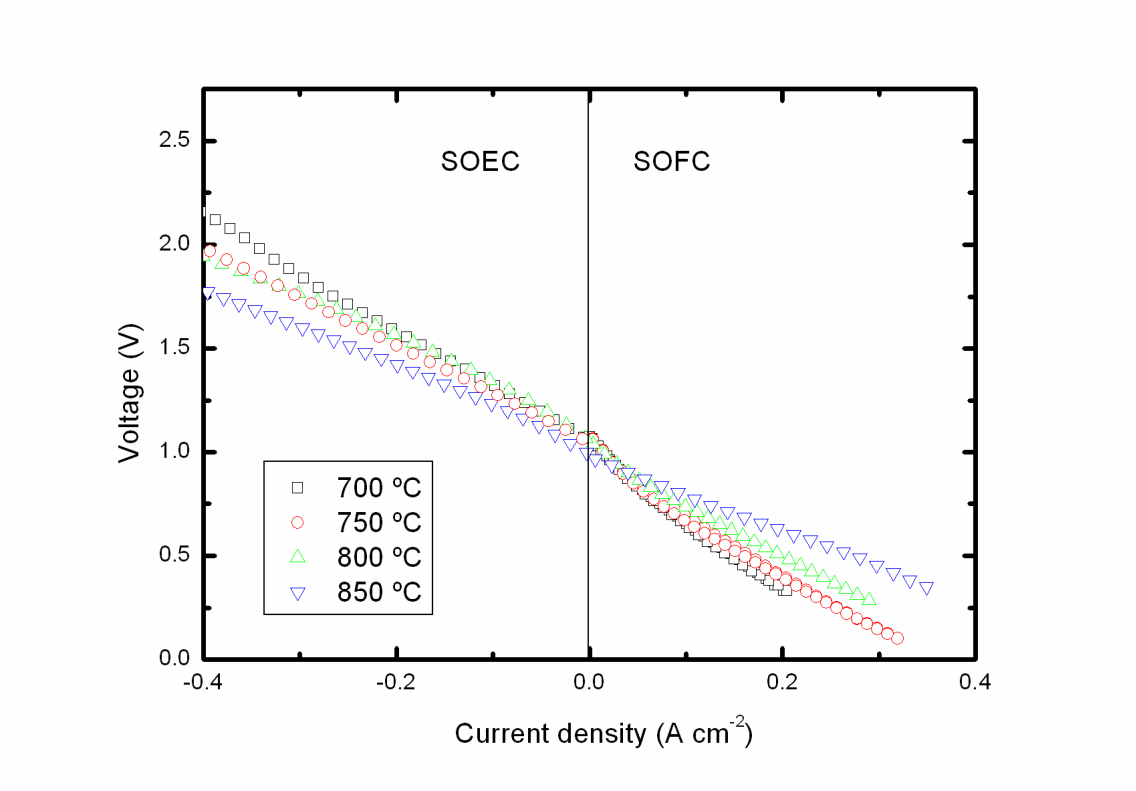
SOEC
SOFC
Voltage (V)
Current density (A cm-2)
700 ºC
750 ºC
800 ºC
850 ºC
2.5
2.0
1.5
1.0
0.5
0.0
-0.4
-0.2
0.0
0.2
0.4

Figure 3

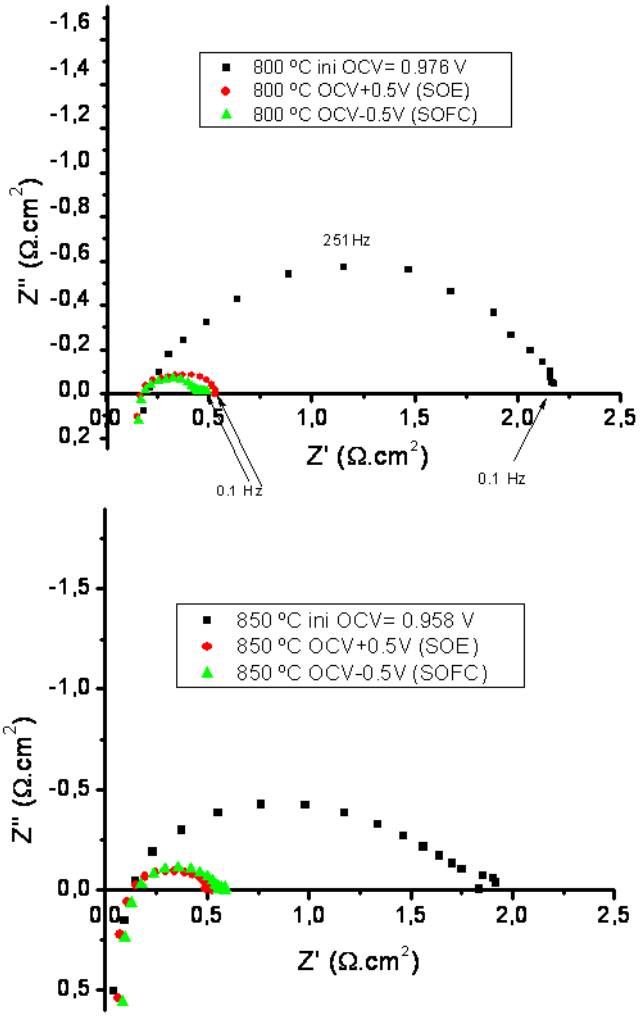
800 °C ini OCV= 0.976 V
800 °C OCV+0.5V (SOE)
800 °C OCV-0.5V (SOFC)
251 Hz
0.1 Hz
0.1 Hz
Z'' (Ω.cm²)
Z' (Ω.cm²)
850 °C ini OCV= 0.958 V
850 °C OCV+0.5V (SOE)
850 °C OCV-0.5V (SOFC)
Z'' (Ω.cm²)
Z' (Ω.cm²)

Figure 4

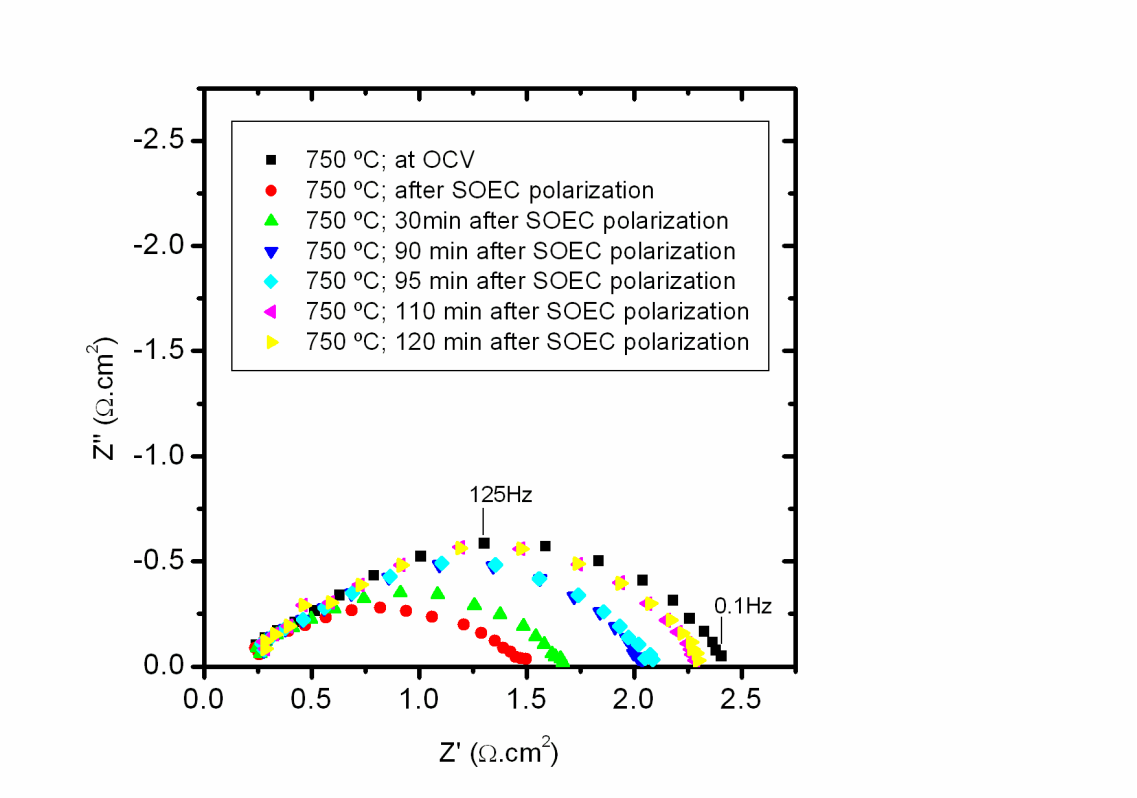

Figure 5

References

[1] S.C. Singhal, K. Kendall (Eds.), High Temperature SOFCs: Fundamentals, Design and Applications, Elsevier, **2003**.
[2] S. J. Skinner and M. A. Laguna-Bercero, Advanced Inorganic Materials for Solid Oxide Fuel Cells, in Energy Materials, Duncan W. Bruce, Richard Walton and Dermot O'Hare (Eds.),Wiley, **2010**.
[3] S. B. Alder, *Chem. Rev.* **2004**, *104*, 4791.
[4] S. J. Skinner, J. A. Kilner, *Solid State Ionics* **2000**, *135*, 709.
[5] J. M. Bassat, P. Odier, A. Villesuzanne, C. Marin, M. Pouchard, *Solid State Ionics* **2004**, *167*, 341.
[6] C. N. Munnings, S. J. Skinner, G. Amow, P. Whitfield, I. Davidson, *Solid State Ionics* **2005**, *176*, 1895.
[7] T. Nakamura, K. Yashiro, K. Sato, J. Mizusaki, *Solid State Ion.* **2009**, *180*, 368.
[8] E.V. Tsipis and V.V. Kharton, *J. Solid State Electrochem.* **2008**, *12*, 1367.
[9] A. A. Yaremchenko, V. V. Kharton, M. V. Patrakeev, J. R. Frade, *J. Mater. Chem.* **2003**, *13*, 1136.
[10] M. L. Fontaine, Ph.D. Thesis, University of Toulouse, France, **2002**.
[11] J. Echigoya, T. Ohfuji, H. Suto, *J. Mater. Sci. Letters* **1994**, *13*, 1098.
[12] G. Amow, P. S. Whitfield, I. J. Davidson, R. P. Hammond, C. N. Munnings, S. J. Skinner, *Ceram. Int.* **2004**, *30*, 1635.
[13] M. A. Laguna-Bercero, S. J. Skinner and J. A. Kilner, A0615, In: U. Bossel, Editor, *Proceedings of 8th European SOFC Forum, The European Solid Oxide Fuel Cell Forum*, **2008**
[14] N. Solak, M. Zinkevich, and F. Aldinger, *Solid State Ionics* **2006**, *177*, 2139.
[15] R. Sayers, J. Liu, B. Rustumji and S.J. Skinner, *Fuel Cells* **2008**, *8*, 338.
[16] H. El Shinawi and C. Greaves, *Z. Anorg. Allg. Chem.* **2009**, *635*, 1856.
[17] H. El Shinawi, J. F. Marco, F. J. Berry and C. Greaves, *J. Solid State Chem.* **2009**, *182*, 2261.
[18] H. El Shinawi and C. Greaves, *J. Solid State Chem.* **2008**, *181*, 2705.
[19] F. Chauveau, J. Mougin, J.M. Bassat, F. Mauvy and J.C. Grenier, *J. Power Sourc.* **2010**, *195*, 744.
[20] V. I. Sharma, B. Yildiz, J. Electrochem. Soc. 2010, 157, B441.

[21] M. S. Sohal, J. E. O'Brien, C. M. Stoots, J. S. Herring, J. Hartvigsen, D. Larsen, S. Elangovan, J. D. Carter, V. I. Sharma, and B. Yildiz, Report no. INL/EXT-09-16004, Report to the U.S. Department of Energy by Idaho National Laboratory, **2009**.
[22] H. El Shinawi and C. Greaves, *J. Mater. Chem.* **2010**, *20*, 504.
[23] J. T. S. Irvine, J. W. L. Dobson, T. Politova, S. García Martín and A. Shenouda, *Faraday Discuss.* **2007**, *134*, 41.
[24] ZView®, Scribner Associates
[25] M. A. Laguna-Bercero, J. A. Kilner and S. J. Skinner, *Chem. Mater.* **2010**, *22*, 1134.
[26] H. El Shinawi, PhD Thesis, University of Birmingham, **2010.**
[27] J. T. S. Irvine, D. C. Sinclair and A. R. West, *Adv. Mater.* **1990**, *2*, 132.
[28] M. Rieu, R. Sayers, M. A. Laguna-Bercero, S. J. Skinner, P. Lenormand and F. Ansart, *J. Electrochem. Soc.* **2010**, *157*, B477.
[29] M. J. Escudero, A. Aguadero, J. A. Alonso, and L. Daza, *J. Electroanal. Chem.* **2007**, *611*, 107..
[30] S. P. Jiang and J. G. Love, *Solid State Ion.* **2003**, *158*, 45.
[31] Y. D. Zhen and San Ping Jiang**,** *J. Electrochem. Soc.* **2006**, *153*, A2245.
[32] F. S. Baumann, J. Maier, J. Fleig, *Solid State Ion.* **2008**, *179*, 1198.